Energy & Environmental Science

ROYAL SOCIETY OF CHEMISTRY

PERSPECTIVE

View Article Online
View Journal | View Issue

Cite this: *Energy Environ. Sci.*, 2025, **18**, 4037

Micro-sized CVD-derived Si–C anodes: challenges, strategies, and prospects for next-generation high-energy lithium-ion batteries

Zhexi Xiao,[ab] Haojun Wu,[ab] Lijiao Quan,[ab] Fanghong Zeng,[cab] Ruoyu Guo,[ab] Zekai Ma,[ab] Xiaoyu Chen,[ab] Jiaqi Zhan,[ab] Kang Xu,*[d] Lidan Xing*[ab] and Weishan Li[ab]

The development of high-capacity anodes is of paramount importance to address the rapidly increasing demand for high-energy-density lithium-ion batteries (LIBs). While the commercialization of nanoscale silicon (Si) and microscale silicon monoxide (SiO) anodes represents a significant milestone, their widespread adoption remains constrained by challenges such as high production costs, severe interfacial side reactions, and substantial initial capacity losses. Recently, a new class of micro-sized Si–C anodes has emerged, fabricated *via* the co-pyrolysis of silane and gaseous hydrocarbons into porous carbon scaffolds using chemical vapor deposition (CVD). These anodes demonstrate promising performance and improved economic viability. However, the unclear mechanisms governing their structural and interfacial evolution pose significant barriers to their practical application. In this perspective, we critically summarize recent advances in understanding the intrinsic phase transition properties and the dynamic evolution of the solid–electrolyte interphase (SEI), with particular emphasis on the "breathing" effect of the SEI during cycling that leads to failure. From both dynamic and static perspectives, we highlight various strategies to address these challenges, especially under demanding conditions such as fast charging and extreme temperatures (high and low). By providing a comprehensive framework for addressing these issues, this perspective aims to offer valuable insights into enhancing the overall performance of this emerging class of anodes and accelerating their industrial adoption.

Received 19th March 2025,
Accepted 7th April 2025

DOI: 10.1039/d5ee01568e

rsc.li/ees

Broader context

The pursuit of high-energy-density lithium-ion batteries (LIBs) is a cornerstone of global efforts to transition toward sustainable energy systems, particularly in electric vehicles (EVs) and grid-scale energy storage. Silicon-based anodes, with their exceptional theoretical capacity, hold immense potential to replace conventional graphite and address the growing demand for energy-dense storage solutions. However, the commercialization of silicon anodes has long been hindered by intrinsic challenges such as severe volume expansion, unstable solid–electrolyte interphase (SEI), and high production costs. The emergence of micro-sized CVD-derived Si–C composites represents a transformative advancement, offering a unique balance of scalability, structural resilience, and electrochemical performance. By embedding nanoscale silicon within porous carbon frameworks, these composites mitigate mechanical degradation and interfacial side reactions while enhancing cycling stability under extreme conditions. This perspective bridges critical gaps between fundamental research and industrial deployment. By elucidating phase transition mechanisms and SEI dynamics, it provides actionable strategies to optimize anode performance for fast-charging and wide-temperature operation as key demands for next-gen EVs and grid storage.

[a] *School of Chemistry, South China Normal University, Guangzhou 510006, China. E-mail: xingld@scnu.edu.cn*
[b] *National and Local Joint Engineering Research Center of MPTES in High Energy and Safety LIBs, Engineering Research Center of MTEES (Ministry of Education), Research Center of BMET (Guangdong Province), and Key Lab. Of ETESPG (GHEI), South China Normal University, Guangzhou 510006, China*
[c] *State Key Laboratory of Luminescent Materials and Devices, School of Materials Science and Engineering, South China University of Technology, Guangzhou 510641, China*
[d] *SES AI Corp., Woburn, MA, 01801, USA. E-mail: kang.xu@ses.ai, kang_xu@hotmail.com*

1. Introduction

High-capacity electrode materials in rechargeable lithium-ion batteries (LIBs) are pivotal to advancing the electrification transition from primary to secondary energy sources.[1–3] Silicon (Si), with its exceptionally high theoretical capacity ($\sim$3580 mA h g^{-1}), has emerged as one of the most promising candidates to replace conventional graphite anodes for next-generation high-energy-density LIBs.[4–6] Despite its potential, the intrinsic limitations of

Si, such as poor electrical conductivity, extensive volume expansion (>300%), and high interfacial reactivity with commercial $LiPF_6$-based electrolytes pose significant challenges to its practical application.[7] Over the past two decades, substantial efforts have been devoted to overcoming these challenges by minimizing the active particle size and incorporating multifunctional buffer matrices.[8–11] Although various nanostructured Si-based anodes have been designed to mitigate some of these issues, their practical deployment is hindered by the high production cost of nanoscale Si, low yield, poor tap density, and high specific surface area, which exacerbates interfacial side reactions and compromises long-term stability.[12–14] In contrast, micro-sized Si materials offer significant advantages in terms of tap density, cost-effectiveness, and reduced specific surface area, which collectively improve volumetric energy density and mitigate interfacial side reactions.[15,16] Nevertheless, for two classical micro-sized Si-based anodes, micro-sized Si anodes exhibit higher internal stress to induce particle fracture and pulverization during the lithiation/delithiation process, and the lengthened transport pathway greatly impede the diffusion efficiency.[17,18] SiO_x ($1 < x < 2$) anode achieved a better tradeoff between volume expansion rate (~160%) and capacity (1600–2400 mA h g^{-1}), but the inactive Li_2O and Li_xSiO_y phase formation during initial lithiation results in low initial coulombic efficiency (ICE), the excess active Li consumption detriments actual energy density and increases treatment cost induced by prelithaition.[19,20]

In recent few years, a novel class of micro-sized Si–C composite particles, first pioneered by Sila Nanotechnologies, has garnered significant attention within the industry. These composites feature a unique structure comprising nanoscale Si encapsulated by carbon, which is formed *via* the co-pyrolysis of silane and gaseous hydrocarbons.[21] The dense carbon coating not only enhances the electrical conductivity of the composite but also provides effective protection for the nanoscale Si. However, achieving uniformity at the nanoscale remains a critical challenge, which has notably hindered further advancements in this technology. At the end of 2022, a major breakthrough in the full-cell performance of Si–C composite anodes developed by Group14 Technologies, as demonstrated by several leading manufacturers, sparked widespread global interest. These next-generation micro-sized Si–C composites are characterized by embedding active nanoscale Si within a low-cost porous carbon skeleton. The porous amorphous carbon framework effectively buffers the volume expansion of Si during lithiation, dissipating internal stress and significantly reducing electrode expansion. This enables high cycling stability and low electrode swelling during operation. Furthermore, the porous carbon skeleton not only provides additional lithium storage capacity but also contributes to the overall energy density of the anode due to its lightweight and cost-effective design.[8,22] In addition to their superior electrochemical performance, these Si–C composites benefit from a streamlined production process with minimal equipment requirements, positioning them as one of the most promising solutions for Si-based anodes in the development of high-energy-density LIBs.[23] However, despite the remarkable progress achieved so far, the question of whether these materials can serve as the ultimate solution for Si-based anodes remains unresolved. With the rapidly increasing demand for LIBs to operate under harsh conditions, such as fast charging and extreme temperature environments, the comprehensive performance of these materials under real-world conditions warrants further in-depth investigation and assessment.

To enhance the comprehensive performance of these micro-sized Si–C composite anodes in practical applications and accelerate their commercialization, this perspective provides a timely and systematic analysis. Starting with a thermodynamic and kinetic examination of the phase transition mechanisms of active silicon, we highlight the critical importance of controlling the internal Si morphology. Understanding these intrinsic mechanisms is essential for optimizing the structural stability and electrochemical performance of the composite anodes. Building on these fundamental insights, we revisit the potential failure mechanisms of these Si–C anodes, drawing on recent advances in the field. Beyond the well-documented volume expansion of bulk Si particles, special emphasis is placed on the "breathing" effect of the solid–electrolyte interphase (SEI), which plays a vital role in both the dynamic and static failure processes. This detailed analysis aims to deepen the understanding of the interplay between volume changes and interfacial instability, which are critical challenges for achieving long-term cycling stability. Based on this mechanistic understanding, we summarize potential strategies for improving the overall performance of these anodes, particularly under demanding conditions such as fast charging and high or low-temperature cycling and storage. These strategies are grouped into two primary categories: internal microstructure optimization and external regulation. For each category, the characteristics, advantages, and limitations of various approaches are discussed in detail, providing a comprehensive framework for addressing the current challenges. Finally, by synthesizing the current research progress on these emerging Si–C composite anodes, we propose potential future directions for their development. This includes a focus on addressing unresolved scientific challenges and identifying pathways for scaling up production to meet industrial demands. By offering these insights, we aim to contribute to the advancement of high-energy-density LIBs and the broader commercialization of this promising class of anode materials.

2. Lithiation mechanisms and structural evolution in crystalline and amorphous silicon

The lithium storage mechanism of silicon, irrespective of its crystalline or amorphous phases, can be generally described by the following reaction:[24]

$$Si + xLi^+ + xe^- \rightarrow Li_xSi \quad (1)$$

However, the lithiation pathways of crystalline silicon (c-Si) and amorphous silicon (a-Si) differ significantly, and these differences play a critical role in influencing the behavior of

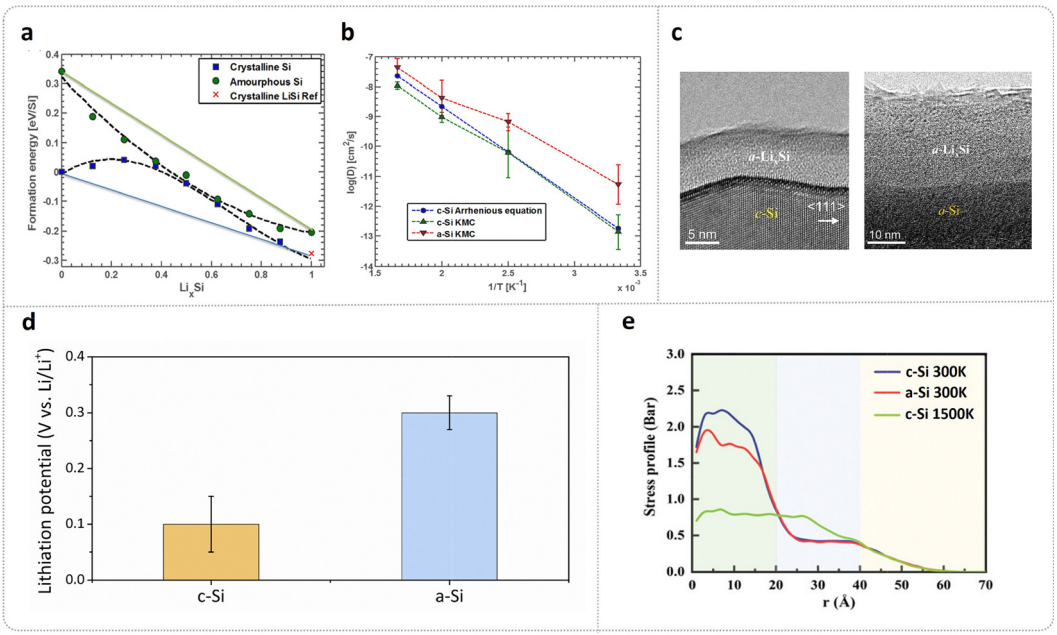

Fig. 1 Phase transition during lithiation for a-Si and c-Si. (a) Formation energies as function of lithiation depth. (b) D_{Li^+} *versus* temperature,[25] with permission from Elsevier, Copyright 2014. (c) TEM observance of phase boundary during lithiation,[26,27] with permission from American Chemical Society, 2013; with permission from Springer Nature, 2012. (d) Statistic analysis of lithiation potential of c-Si and a-Si. (e) The stress during lithiation,[28] with permission from Wiley-VCH, 2023.

the carbon skeleton (guest matrix), ultimately affecting the overall performance and cycle life of the anode.

From a thermodynamic perspective, as illustrated in Fig. 1a, the lithiation of c-Si and a-Si exhibits distinct characteristics due to differing thermodynamic driving forces. For c-Si, the initial insertion of lithium is thermodynamically unfavorable, leading to phase separation between c-Si and the lithiated amorphous silicon (a-Li$_x$Si). In contrast, the lithiation of a-Si proceeds uniformly, driven by the stable growth of a-Li$_x$Si alloy phase. This fundamental difference in phase transition behavior has profound implications for the structural integrity and stress evolution of the Si-based composite anodes. From a kinetic perspective, these differences are further highlighted by the lithium diffusion coefficients (D_{Li^+}) in c-Si and a-Si at room temperature. Simulation studies indicate that the D_{Li^+} value in c-Si is approximately 10^{-13} cm^2 s^{-1}, while the average D_{Li^+} in a-Si is approximately 10^{-11} cm^2 s^{-1}, indicating that lithium diffusion in a-Si is at least an order of magnitude faster than in c-Si (as shown in Fig. 1b).[25] This disparity underscores the superior lithiation kinetics of a-Si, making it more favorable for applications requiring rapid charge and discharge rates.

In situ high-resolution TEM experiments have provided insights into the two-phase lithiation mechanism of c-Si, as presented in Fig. 1c. The lithiation process involves the formation of an amorphous Li$_x$Si layer at the c-Si surface, followed by a sharp amorphous interface movement facilitated by layer-by-layer ledge flow at the interface. In contrast, the atomic structure of a-Si, characterized by a continuous random network of Si atoms without long-range order, leads to a more homogeneous lithiation pathway. Although the local bonding environment in a-Si resembles that of c-Si, the amorphous–amorphous phase boundary allows lithium atoms to aggregate more readily, weakening the covalent bonds between Si atoms and promoting lithiation at room temperature. This results in the formation of a less well-defined phase boundary, further enhancing the lithiation kinetics.[26,27] Despite these differences, both a-Si and c-Si share a fundamental challenge: the strong covalent bonding energy of Si–Si. This characteristic makes it inherently difficult to disrupt the covalent silicon network, resulting in a relatively low rate of Si dissociation from the network at room temperature. Overcoming this intrinsic limitation remains a critical consideration for improving the lithiation efficiency and overall performance of Si-based anodes.

An analysis of lithiation potentials reported in the literature reveals that the lithiation potential of c-Si is approximately 0.2 V lower than that of a-Si (Fig. 1d).[29–33] This difference in voltage plateaus is closely related to the distinct microstructural evolution of c-Si and a-Si during lithiation, which in turn influences the electrode's kinetic behavior and stress distribution.

For a-Si, the average coordination number of Si–Si steadily decreases from 3.8 to 0.5 as lithiation progresses, indicating a gradual and uniform breakup of Si–Si bonds. In contrast, for c-Si, the initial lithiation mechanism is markedly different. During the early stages, lithium ions randomly insert into the silicon cluster cavities within the crystalline lattice, forming a solid solution of Li–Si. During this phase, the Si network remains largely intact. As lithiation proceeds (x = 0.065), the Si–Si bonds begin to break, and the long-range crystalline order gradually disappears, transforming the structure from a crystalline phase to an amorphous phase characterized by distorted Si tetrahedrons. This phase transition in c-Si is accompanied by significant lithium concentration heterogeneity and the

generation of higher internal stress, particularly during the early stages of lithiation (Fig. 1e). The higher stress levels in c-Si indicate unfavorable thermodynamic conditions for lithium insertion, as evidenced by the higher formation energy required for Li insertion compared to a-Si. In contrast, a-Si exhibits a more uniform lithiation process with lower internal stress. The reduced stress in a-Si, coupled with its higher lithium diffusivity, underscores its superior resistance to fracture and enhanced capacity delivery during cycling. These characteristics make a-Si a more promising candidate for Si-based anodes, particularly in applications requiring high stability and robust electrochemical performance.[28]

3. Latest advances in understanding dynamic and static failure mechanisms in micro-sized Si–C anodes

To better understand the failure mechanisms of micro-sized chemical vapor deposition (CVD)-derived Si–C anodes, it is essential to investigate both dynamic and static aspects of their degradation. One of the primary challenges in Si–C anodes arises from the substantial volume changes of silicon during lithiation and delithiation, which manifest as pulverization, particle cracking, and interfacial debonding at the particle level.[34–36] Beyond this well-documented issue, recent studies have highlighted the role of the SEI in the degradation of Si–C anodes. Unlike graphite anodes, silicon-based anodes exhibit an intrinsically non-passivating SEI, which undergoes continuous dynamic evolution during cycling.[37]

A critical aspect of the SEI evolution is its mechanical instability, often referred to as the ''breathing'' effect. As shown in Fig. 2a, the parasitic current caused by electrolyte reduction does not drop to zero during the lithiation/delithiation processes, regardless of whether the SEI is deformed. However, the parasitic current increases significantly when the SEI is mechanically deformed, which can be attributed to both its inherent non-passivating behavior and strain-induced mechanical effects. During lithiation, the SEI layer is stretched, generating tensile strain that results in localized loosening of its structure and morphology. This deformation creates small channels and voids, allowing ethyl methyl carbonate (EMC) or solvated Li^+ ions to penetrate the SEI and react with the underlying silicon surface, leading to localized electroreduction of the electrolyte. Upon delithiation, the SEI contracts, trapping EMC and soluble decomposition products within its structure.[38] Fig. 2b provides visual evidence of these failure mechanisms in micro-sized Si–C anodes within pouch cells. The decomposition of organic electrolyte components and the formation of amorphous $Li_2Si_xO_\gamma$ compounds promote gradual SEI porosification during cycling. This porosification allows the electrolyte to permeate the SEI, enabling continuous reactions with bulk silicon. Consequently, the SEI grows in a bottom-up manner due to reactions at the Si surface. Simultaneously, electron penetration into the SEI induces top–down decomposition, further thickening the SEI. The gigapascal-scale stress generated during silicon alloying punctures the SEI, disrupting the structural integrity of the electrode. As the SEI thickens, it compromises the percolation pathways between active particles and the conductive agents, leading to severe electrical contact loss and the formation of electrically isolated ''dead silicon'', which contributes to rapid capacity decay and lithium inventory loss (Fig. 2c).[4,39–41] The local electrical degradation of Si–C anodes has been further characterized using scanning spreading resistance microscopy (SSRM) at nanoscale resolution (Fig. 2d). This technique reveals a significant increase in local resistivity within the electrode after cycling, clearly demonstrating that continuous SEI aging damages the conductive network within the active particles.[42] This loss of electrical connectivity, combined with the dynamic evolution of the SEI, underscores the critical need for strategies to stabilize the SEI and maintain the conductive network to improve the long-term performance of Si–C anodes.

During the aging of the SEI, special attention must be given to the emergence of parasitic currents, which signify the loss of lithium inventory (LLI), electrolyte consumption, and gas generation. These factors are closely linked to the failure of Si-based anode batteries during calendar aging.[48] Calendar aging refers to the time-dependent performance degradation of batteries even in the absence of cycling.[49] For Si-based anodes, calendar aging is more severe than for graphite anodes, as it involves not only LLI but also significant loss of active material (LAM) and chemical instability.[50] These issues contribute to a higher self-discharge rate and insufficient calendar life, making Si-based anodes particularly susceptible to long-term degradation. As previously mentioned, the properties of the SEI play a critical role in determining the calendar aging behavior of batteries. Regulating the uniformity of the SEI, particularly its composition and spatial distribution, has been shown to effectively reduce electron leakage. This decreases the driving force for SEI growth and enhances its electron-insulating properties, thereby mitigating aging processes (Fig. 2e).[44] However, for Si–C anodes, managing electron transport behavior remains a significant challenge, as the presence of silicon accelerates electron transitions between phases.

During high-temperature storage, time-of-flight secondary ion mass spectrometry (TOF-SIMS) combined with scanning transmission electron microscopy-electron energy loss spectroscopy (STEM-EELS) reveals that SEI thickening is accompanied by the formation of a high lithium concentration gradient on the particle surface. This gradient not only leads to continuous LLI but also induces large local stresses, further exacerbating degradation (Fig. 2f).[45] The evolution of Si–C anodes during storage is illustrated in Fig. 2g and h. Self-discharge occurs on both carbon and silicon, but the rate is highly dependent on the intrinsic stability of the SEI. Unlike the stable SEI on graphite, the SEI on silicon is inherently unstable, lacking the ability to effectively passivate electron transfer to the electrolyte due to high surface work function of silicon.[46] At elevated temperatures, only the electron energy levels of silicon decay, creating an instantaneous energy gap between the silicon and graphite phases. This gap is subsequently moderated by spontaneous electron transfer. Silicon accepts electrons directly from graphite

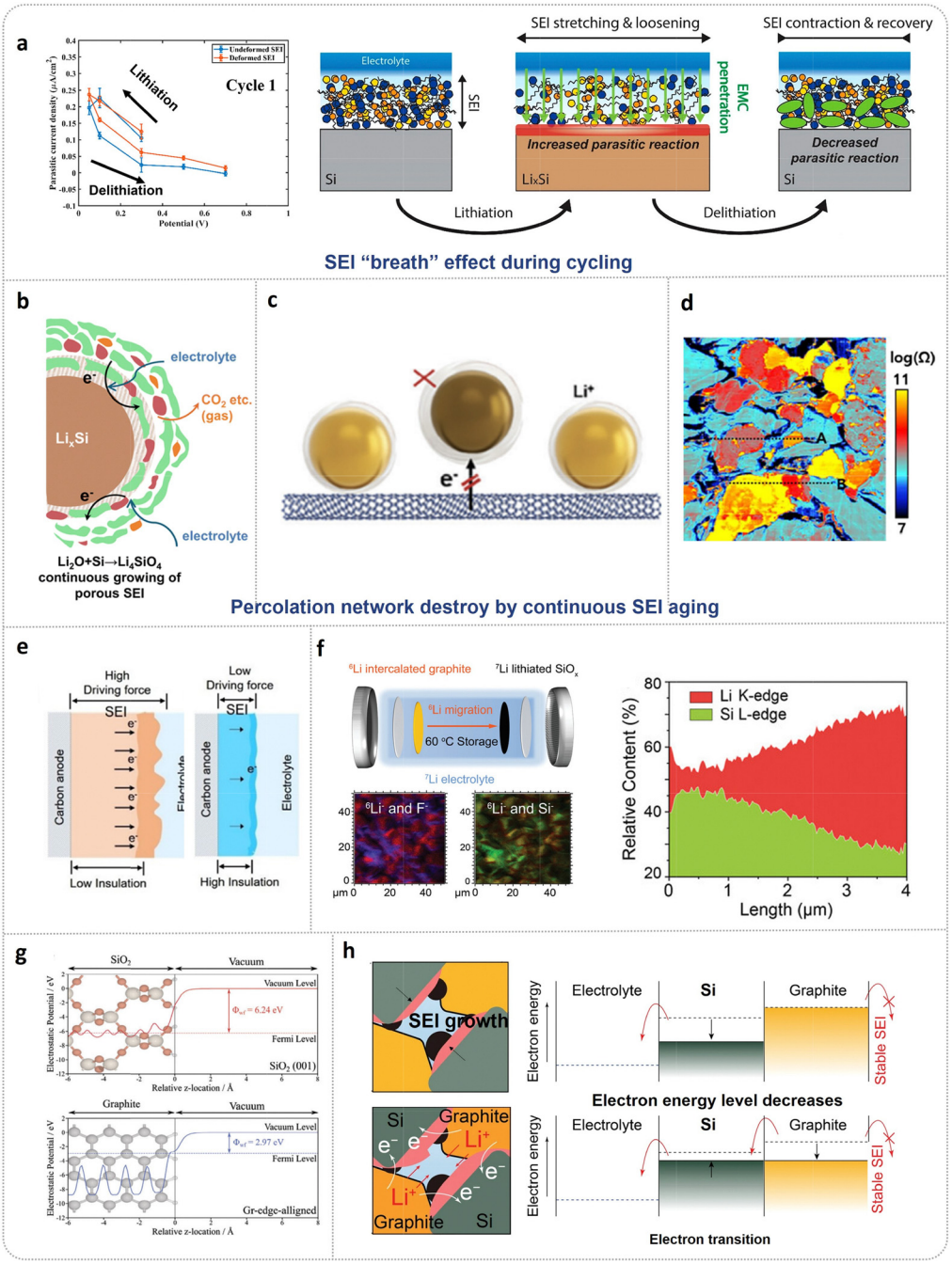

Fig. 2 Dynamic and static failure mechanism of Si–C anodes. (a) SEI dynamic breath effect,[38] with permission from American Chemical Society, 2023. (b) SEI structure after cycling,[43] with permission from Royal Society of Chemistry, 2024. (c) Percolation network destroy due to mechanical stress,[4] with permission from Wiley-VCH, 2024. (d) Electrical contact loss during cycling,[42] with permission from American Chemical Society, 2018. (e) Electron leakage in SEI,[44] with permission from Wiley-VCH, 2023. (f) Short circuit coin cell consisted of ^{6}Li to monitor the lithium migration at 60 °C calendar aging and corresponding TOF-SIMS and STEM-EELS images,[45] with permission from Wiley-VCH, 2024. (g) Surface work function of Si and graphite anodes,[46] with permission from Wiley-VCH, 2023. (h) Electronic transition during HT storage of high SOC Si–C composite anode,[47] with permission from Springer Nature, 2023.

while simultaneously accepting lithium ions from the electrolyte to balance the energy level difference. This process is accompanied by lithium leaching from graphite, driven by continuous electron transfer from carbon to silicon.[47] The result is a persistent cycle of electron leakage and lithium redistribution, which further destabilizes the SEI and accelerates performance degradation.

Given these challenges, constructing an artificial SEI with optimized properties is of paramount importance. Whether through surface modification of the active material or regulation of the solvation structure from the electrolyte perspective, these strategies are critical for addressing calendar aging. By mitigating electronic energy level imbalances and stabilizing the SEI, such approaches can significantly

enhance the long-term stability and performance of Si–C anodes.

4. Potential strategies for improving the performance of micro-sized CVD derived Si–C anodes

4.1 Internal microstructural control

4.1.1 Nucleation restraint. The performance of micro-sized CVD-derived Si–C anodes is critically dependent on the design of the carbon framework and the conditions for silicon deposition, as these factors directly influence volume expansion behavior and ion/electron diffusion efficiency. For the silicon deposition process, controlling the reaction conditions is particularly important for regulating the internal particle phase. Typically, the optimal reaction temperature ranges between 400–600 °C. At lower temperatures, the decomposition of the carbon source is insufficient, reducing process efficiency, whereas higher temperatures promote crystallization and excessive nucleus growth, which negatively impacts cycling performance. However, achieving precise control of nano- or subnano-scale silicon deposition within the carbon skeleton remains a significant challenge in this temperature range.

During the thermal decomposition of monosilane gas (SiH_4), silicon particles grow continuously due to uncontrolled nucleation processes. Inhibiting this growth during nucleation is critical to forming fine silicon particles ($\sim$1 nm). As shown in Fig. 3a, density functional theory (DFT) calculations reveal that the SiH_3 radical, produced from SiH_4 decomposition, preferentially reacts with ethylene (C_2H_4) rather than monosilane.[51] The presence of ethylene promotes the formation of Si–C bonds, disrupting the continuous growth of silicon nuclei and resulting in subnano-scale silicon encapsulated within a SiC/a-C matrix. In contrast, using pure SiH_4 without ethylene leads to uncontrolled Si–Si bond formation and larger silicon particles. As the SiH_4-to-C_2H_4 ratio increases from 10 : 0 to 10 : 5, X-ray diffraction (XRD) results show a reduction in silicon grain size from 40 nm to 0.87 nm. This indicates that carbon atoms adsorbed on the silicon surface significantly suppress Si–Si bond formation and inhibit silicon cluster growth. By leveraging ethylene as a growth inhibitor, subnano-scale silicon crystals can be embedded into a porous carbon substrate, which enhances structural stability during repeated lithiation/delithiation cycles due to their high structural reversibility and low strain.

The practical feasibility of such anodes has been verified in large-scale applications. A 107 kW h battery pack composed of 110 A h full-cells with these anodes demonstrated excellent cyclic stability (91% capacity retention over 2875 cycles) and calendar life (97.6% capacity retention over one year). These results highlight the potential of this approach for commercial applications.

4.1.2 Si/C interphase regulation. The regulation of the Si/C interphase within the carbon framework plays a multifunctional role in improving overall performance. Interfacial silicon carbide (SiC) not only controls the growth of silicon crystals but also enhances oxidation resistance, preventing the formation of an inert SiO_2 layer during high-temperature processes. This helps suppress ICE loss and capacity fade.[56] Moreover, edge carbon atoms within the carbon framework exhibit higher adsorption energies, which strengthen interactions with embedded active components such as silicon or phosphorus atoms. These robust interactions facilitate the formation of stable Si–C or P–C bonds, stabilizing structural changes in the composite under fast cycling conditions.[57,58]

By controlling the crystallographic orientation of the carbon substrate, SiC can be induced to form at the open edges of carbon nanotubes (OCNTs). This strengthens the bonding between silicon and the carbon matrix, effectively reducing interfacial mechanical detachment caused by high internal stress. DFT and reactive molecular dynamics (RMD) simulations of interfacial ionic transport show that at high states of charge (SOC), lithium enrichment at the interface generates tensile stress, leading to interfacial delamination and cracking (Fig. 3b). However, the presence of SiC mitigates this effect by reducing the amount of lithium diffusing to the SiC region. The carbon network dissociating from SiC dissipates tensile stress and preserves the dynamic connection between silicon and the carbon substrate, inhibiting interfacial delamination.[52,59]

Beyond mechanical stabilization, SiC also acts as an artificial protective layer against interfacial side reactions. A dense SiC coating ($\sim$5 nm thick) can selectively permeate lithium ions while preventing contact between PF_6^- and active silicon (Fig. 3c). Using an *in situ* by-product analysis system, we identified the core side reaction product, Li_2SiF_6, generated under different reaction temperatures. The activation energy of this reaction was found to be 10% higher with SiC protection, revealing that SiC significantly enhances resistance to side reactions and PF_6^- corrosion. The side reaction rate is reduced by 300-fold, stabilizing cyclic performance.[53]

However, the presence of SiC is not universally beneficial. Due to its inherent electrochemical inertness, excessive SiC thickness hinders lithium-ion diffusion, reducing energy density and adversely affecting capacity and rate performance. Recent studies on the structure–activity relationship of SiC content reveal that the lithium diffusion energy barrier in SiC_4 units formed at high temperatures is more than three times higher than that of pure silicon (Fig. 3d).[54] Excessively high reaction temperatures or C_2H_4 concentrations promote the formation of a SiC_4-rich surface layer, which slows lithiation kinetics and increases interfacial impedance. This highlights the dual nature of SiC: while it improves mechanical stability and side reaction resistance, it can also detrimentally impact capacity and dynamic properties if improperly regulated. Future research should focus on optimizing reaction conditions to balance these effects.

4.1.3 Gradient nano-silicon embedding and carbon skeleton optimization. Recent advancements in micro-sized CVD-derived Si–C anodes have increasingly emphasized the importance of gradient nano-silicon embedding. As shown in Fig. 3e, compared to earlier anodes (*e.g.*, SCC55™ from Group14 Technology), emerging designs from companies such as Huawei and

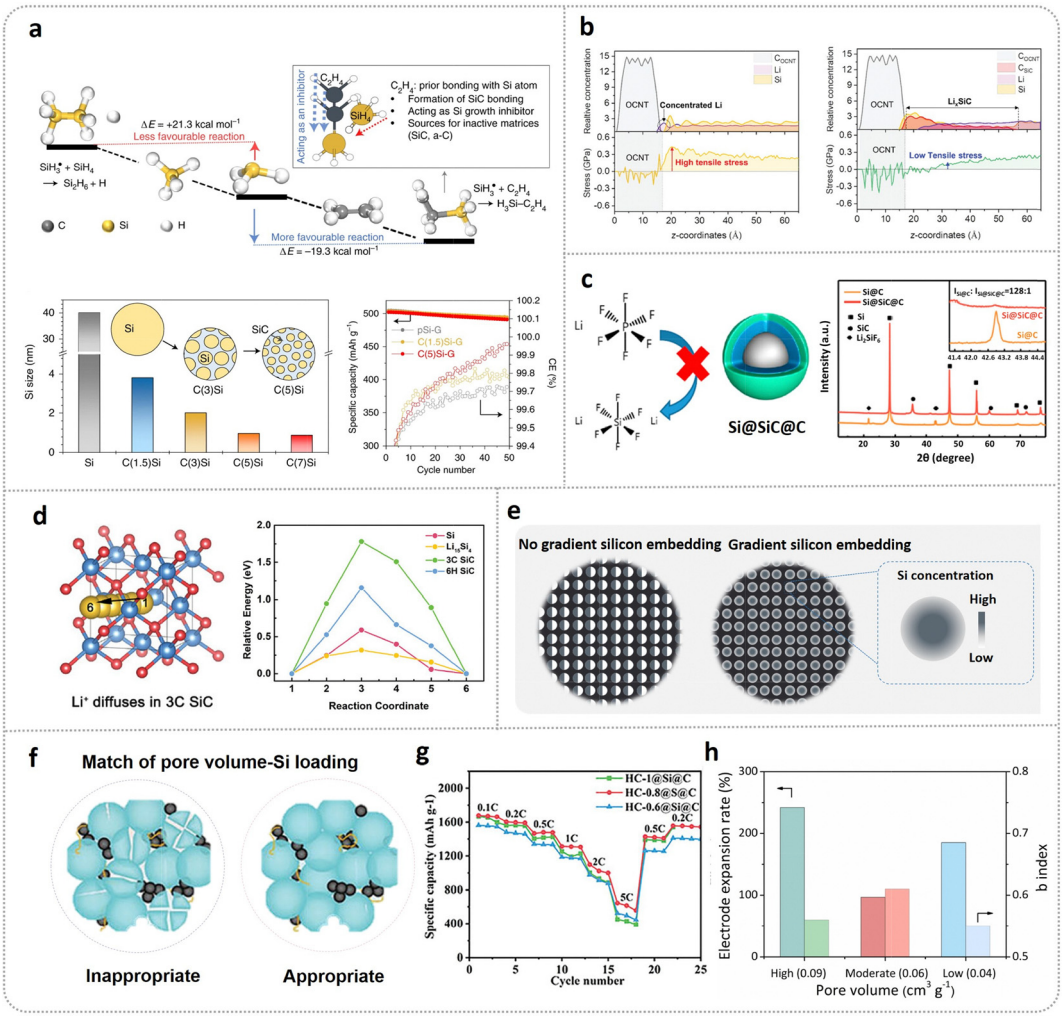

Fig. 3 Internal microstructure control strategies for promoting CVD-drived micro-sized Si–C anodes. (a) Reaction control in SiH_4 deposition: ethylene gas promotes SiC formation to inhibit the Si growth,[51] with permission from Springer Nature, 2021. (b) The effect of SiC formation in distributing the Li^+ concentration at interface to suppress lithiation stress,[52] with permission from Wiley-VCH, 2023. (c) SiC as artifical protective layer to block interfacial side reaction,[53] with permission from American Chemical Society, 2019. (d) The relationship between interfacial SiC_4 and Li^+ diffusion,[54] with permission from Wiley-VCH, 2024. (e) Gradient Si design in porous carbon substrate. The importance of match of pore volume in porous carbon substrate with Si loading: (f) different match of pore volume to Si active particles, (g) its effect on rate performance and (h) electrode expansion rate/*b* index *versus* pore volume,[55] with permission from Wiley-VCH, 2024.

BYD have adopted gradient structures to fill the pores in the carbon substrate.[22] This approach involves introducing a mixed gas containing silane (*e.g.*, SiH_4, ethylsilane, silicon chloride) and carbon source gases (*e.g.*, acetylene, methane, ethylene) during the pyrolysis process. The composition of the mixed gas is dynamically adjusted, with the concentration of silane gradually decreasing as the reaction proceeds, while the carbon source gas concentration increases. This process enables nano-sized silicon to form inside the porous carbon substrate, exhibiting a gradient distribution with a Si-rich core and Si-poor outer layer. The gradient structure design has been successfully applied to core–shell and other composite architectures.[60–62] This Si-rich inside/Si-poor outside configuration effectively reduces stress concentration within the silicon particles during lithiation, mitigating internal stress-induced crack formation and interfacial debonding.[63] Such designs are particularly beneficial for improving the mechanical and electrochemical stability of Si–C anodes during long-term cycling.

In terms of the carbon skeleton, controlling the average particle size is critical, with the ideal size range being 4–6 μm. Excessively small particles can lead to silicon aggregation on the substrate surface, resulting in uneven distribution, while larger particles increase bulk diffusion resistance. However, optimizing the overall particle size alone is insufficient. Previous carbon skeleton designs have primarily focused on the overall structural framework, often neglecting the optimization of internal pathways for ion and electron transport. To improve conductive efficiency, it is essential to increase the contact area between the conductive framework and the active phase while minimizing transport distances. A layered framework composed of wood-derived carbon (WDC) and highly cross-linked carbon nanotubes (CNTs) has been found to reduce electrode curvature,

thereby enhancing ion diffusion and electron conduction.[64] This framework also provides a stable platform for active particle loading, offering valuable insights for future carbon skeleton design in micro-sized CVD-derived Si–C anodes.

Despite these advances, the significant volumetric expansion of silicon during cycling remains a substantial challenge. The use of carbon-based matrixes, such as graphite flakes, carbon nanotube cages, offers a potential solution by providing sufficient space to accommodate this expansion, while their abundant sub-nanometer microchannels enhance composite conductivity. Recently, a high-performance micro-sized Si/C composite anode is prepared by combining spray drying of commercial graphite flakes and nanosilicon particles with a CVD process. The vertical growth of thin graphene nanosheets establishes a robust conductive network within internal pores, which can effectively buffer the volume expansion of nanoscale Si while ensuring the internal conductive network integrity, to enable the stable cycling even at high areal loading.[65] Given the common issues of high volume change and poor conductivity in silicon-based and phosphorus-based anodes, similar approach has also been applied in red phosphorus anodes, where nanoscale red phosphorus was integrated into carbon nanotube cages (CNCs) using phosphine treatment combined with a gas-filling method.[66] This strategy effectively addresses the issues of volume expansion and poor conductivity in red phosphorus anodes to achieve a better cyclability with improved rate capability. The development of novel carbon frameworks or composite strategies remains crucial for further advancing internal skeleton regulation in these anodes.

The regulation of pore volume, pore size, and porosity within the carbon substrate, as well as their compatibility with the amount of deposited silicon, plays a pivotal role in determining integral performance. Pore volume not only affects silicon loading but also significantly influences structural stability and mechanical properties. Low pore volume cannot support high silicon loading, leading to interfacial silicon enrichment, while high pore volume compromises mechanical robustness. Both scenarios are detrimental to achieving long cycle life and high rate performance. The effect of pore volume on performance demonstrates that an appropriate match between pore volume and silicon deposition is critical. This balance results in lower electrode expansion rates, enhanced dynamic properties, and improved rate performance, as shown in Fig. 3f–h.[55] A high proportion of micropores in the carbon skeleton can limit the continuous growth and agglomeration of nano-sized silicon, ensuring high electronic and ionic transport efficiency. However, the porosity of the carbon skeleton also affects its mechanical strength. The requirements for pore volume, pore size, and porosity vary significantly depending on specific application scenarios and must be carefully optimized.

Recently, the introduction of heteroatoms into the carbon skeleton has emerged as a promising strategy to further optimize the internal structure of micro-sized CVD-derived Si–C anodes.[67] Drawing inspiration from red phosphorus anodes, which also experience substantial volumetric expansion, nitrogen-doped carbon networks or sulfur–nitrogen co-doped carbon nanofibers have been shown to effectively stabilize red phosphorus particles and mitigate structural damage caused by expansion.[68,69] Similarly, in Si–C anodes, the incorporation of heteroatoms enhances the interaction between the active silicon phase and the substrate by forming stronger covalent bonds. This improves binding strength and stabilizes the internal structure of the composite material, particularly during cycling.

However, heteroatom doping also introduces challenges by increasing process complexity. The potential negative effects of doping on ionic and electronic conductivity require further investigation to fully understand its impact on performance. Balancing the benefits of heteroatom doping against the associated trade-offs is essential for optimizing the design of Si–C anodes.

4.2 External regulation

In addition to the internal microstructural optimization of micro-sized CVD-derived Si–C anodes, significant efforts have been devoted to improving their integral performance through external regulation strategies. These strategies include surface modification, electrolyte interfacial engineering, conductive network design, and the development of functional binders. In this section, we summarize and evaluate key advancements in external regulation, aiming to stimulate the development of efficient and industrially viable extrinsic adjustment technologies to comprehensively enhance the performance of micro-sized CVD-derived Si–C anodes.

4.2.1 Ideal artificial SEI construction. The construction of an ideal SEI at the electrode/electrolyte interface is critical for achieving superior rate performance in Si-based anodes. Extensive research has been conducted from both the coating material and electrolyte perspectives to build an SEI layer that improves electrochemical performance. For micro-sized Si–C anodes, the SEI must not only exhibit mechanical robustness to accommodate the substantial volume expansion of silicon during cycling but also enable rapid Li^+ migration through the interphase to enhance rate capability.

Functional coating layers have emerged as an effective approach to precisely regulate the interfacial chemistry of the SEI, enabling improvements in both mechanical and ionic properties. As shown in Fig. 4a, phosphorus-based (P-based) coating layers have been demonstrated to enhance the adsorption of fluoroethylene carbonate (FEC) in the electrolyte, promoting the formation of an SEI enriched with inorganic components. Cryo-electron microscopy (Cryo-TEM) reveals that this SEI contains abundant LiF and Li_3P, dual inorganic components that exhibit excellent mechanical stability. The presence of Li_3P significantly enhances interfacial ionic conductivity by reducing the diffusion energy barrier for Li^+ migration through the SEI. This results in improved rate performance, achieving a capacity retention rate of 82.7% under a high charge rate of 3C.[70]

For the micro-sized CVD-derived Si–C anodes, after incorporating nano-Si into a porous carbon matrix, a carbon coating

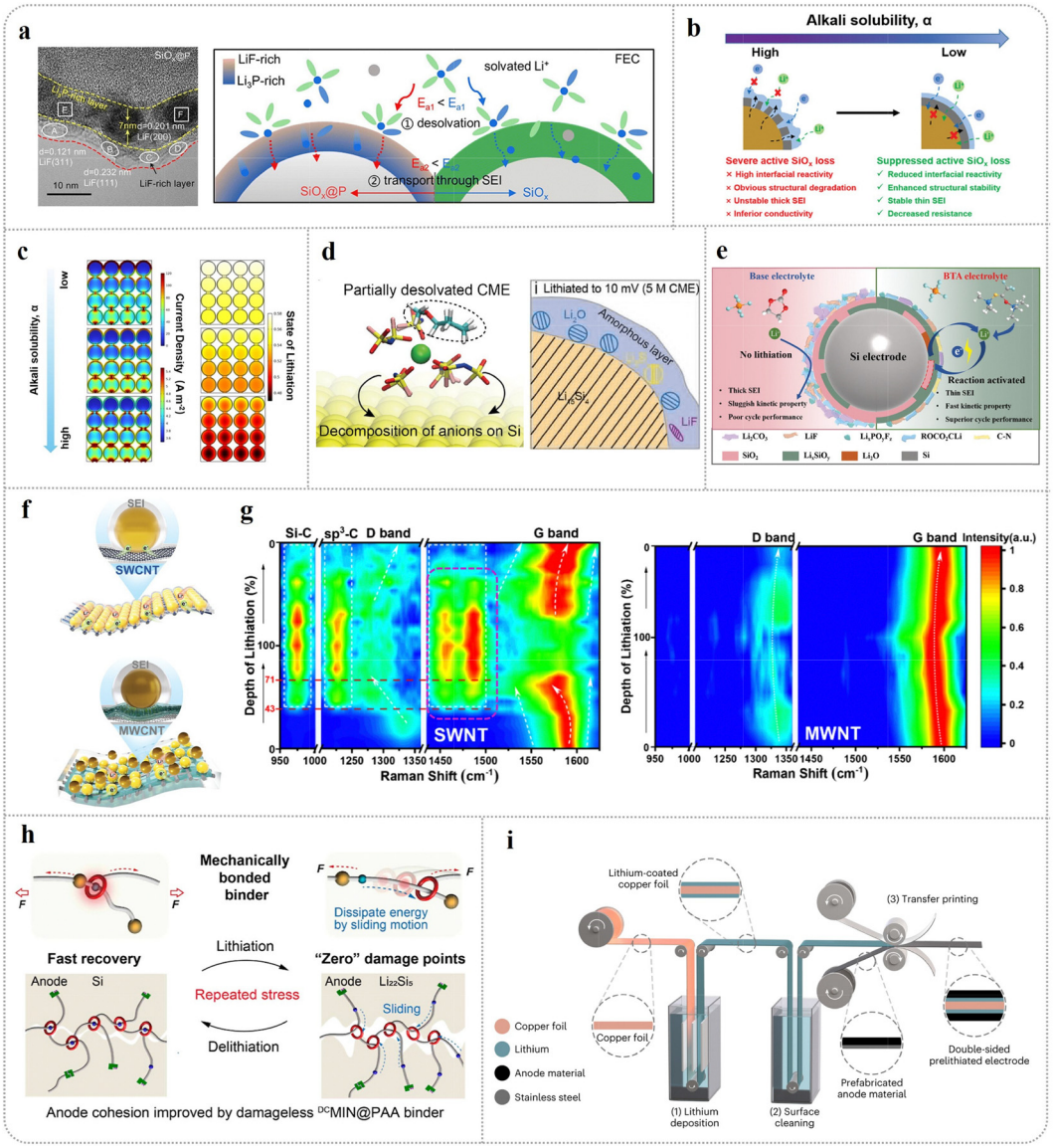

Fig. 4 External regulation strategies. (a) P-based coating layer facilitates the formation of a robust, thin, and dense Li_3P/LiF-dominant SEI,[70] with permission from Royal Society of Chemistry, 2024. The significance of alkali coating integrity: the effect of alkali solubility on (b) interfacial reaction failure,[71] with permission from Wiley-VCH, 2023 and (c) state of lithiation and exchange current density under fast charging,[72] with permission from Springer Nature, 2024. (d) LHCE design with weak solvation structure,[73] with permission from Wiley-VCH, 2024. (e) BTA additive in regulating the structure and composition of the SEI of Si anode,[74] with permission from Wiley-VCH, 2025. (f) Contact mode difference after cycling between SWCNT and MWCNT as conductive network in stabilizing Si–C anodes, and (g) corresponding *in situ* Raman spectra during initial cycling,[39,75] with permission from Wiley-VCH, 2023; with permission from American Chemical Society, 2024. (h) Sliding design of fast recovery and zero damage of mechanically bonded binder,[76] with permission from American Chemical Society, 2024. (i) Thin layer preliathiation technique,[77] with permission from Springer Nature, 2023.

is introduced to enhance overall electrical conductivity and prevent direct contact between the active silicon and the electrolyte, thereby inhibiting side reactions. The integrity of the carbon coating is crucial for performance; inadequate coating integrity can lead to significant dissolution of active Si, resulting in severe interfacial degradation and pronounced lithiation inhomogeneity during fast charging (Fig. 4b and c).[71,72] To address these challenges, fluidized-bed chemical vapor deposition (FBCVD) has emerged as a widely adopted solution in both academic research and industrial applications. FBCVD offers high mass and heat transfer efficiency, coupled with strong two-phase turbulence, which effectively prevents the formation of reaction dead zones and ensures uniform carbon coating integrity.[10] However, quantitatively assessing the integrity of the carbon coating remains a critical challenge. Recent advancements have introduced a selective alkali solution method, which has demonstrated high operability and feasibility for industrial-scale, high-efficiency testing. This method provides a reliable approach for evaluating the quality of carbon coatings and ensuring their effectiveness in practical applications.[71]

To meet the growing demand for stable operation of high-energy-density LIBs across a wide temperature range, electrolyte engineering has emerged as a critical strategy for tailoring the SEI chemistry and structure by precisely regulating the solvation environment.[78,79] For Si-based anodes, which face unique challenges under extreme conditions, the solvation structure must be carefully optimized. At low temperatures, interfacial sluggish transport kinetics significantly increase the diffusion energy barrier, while at high temperatures, aggravated parasitic reactions accelerate capacity decay.[80,81] These issues underscore the need for advanced electrolyte systems designed to stabilize Si-based anodes in real-world applications.

FEC is widely recognized as an effective film-forming additive for improving cyclic stability. However, under extreme temperature conditions, FEC does not always provide positive results. At high temperatures, it can exacerbate active material corrosion due to the formation of hydrofluoric acid (HF), which accelerates capacity degradation.[82–84] This limitation highlights the necessity of developing new electrolyte systems capable of ensuring stable operation over a broad temperature range. Cycloamyl methyl ether (CME) possesses advantages such as low density, a broad liquid phase range, and a moderate dielectric constant. Its weak solvation capability facilitates the formation of a double-layered SEI structure characterized by uniformly dispersed internal inorganic nanoclusters, which is fully encapsulated by external amorphous layers. This structure distinctly differs from the granular LiF formed through FEC decomposition during the initial cycle. The application of an external electric field further enhances the interphasial performance by promoting the migration of Li^+ towards the Si anode interface. Due to the strong cohesive cation–anion association, bis(fluorosulfonyl)imide (FSI^-) anions accumulate near the interface, which reduces the number of solvent molecules in the inner Helmholtz plane (IHP) (Fig. 4d). This weak solvation structure enables stable discharge capacities of 1000 mA h g^{-1} at −20 °C and improves cyclic stability at high temperatures by eliminating FEC from the electrolyte.[73] Beyond CME, other weak solvation structure designs, such as localized high-concentration electrolytes (LHCEs), have also shown promise. The primary goal of LHCEs is to enhance the desolvation kinetics of Li^+, promoting the reduction of anions and facilitating the formation of inorganic-rich SEI layers. These SEI layers provide improved mechanical robustness and electrochemical stability, which are essential for maintaining performance under challenging conditions.[85–87]

The development of novel electrolyte additives has proven effective in further optimizing the interfacial SEI structure, which is crucial for enhancing the performance and stability of Si-based anodes. As shown in Fig. 4e, bis(trimethylsilyl) trifluoroacetamide (BTA), a newly developed electrolyte additive, can actively remove the intrinsic inert SiO_2 layer on the silicon surface. This process significantly reduces electrochemical polarization and enhances Li^+ transport, thereby improving the overall electrochemical performance.[74] The ether system demonstrates superior capability in suppressing gas generation in silicon-based batteries compared to the ester system, making them more suitable for high-performance applications.[88,89] In particular, the incorporation of perfluoroether additives with functional groups such as sulfonyl fluorides or trifluorovinyl ethers within locally superconcentrated electrolytes (LSCE) has shown remarkable results. These additives exhibit preferential reactivity with silicon, promoting the formation of an inorganic-rich SEI layer linked to their reactive functional groups. Perfluoroether additives containing sulfonyl fluoride offer significant advantages due to their unique topology, which enhances anchoring efficiency and provides tether flexibility between anchoring sites. This design improves SEI resiliency by mitigating delamination, reconstitution, and dissolution kinetics. As a result, the total battery capacity retention rate can be increased by up to 45%.[88]

For the ideal artificial SEI construction for micro-sized CVD Si–C anodes, where the nanoscale silicon domain typically consists of both c-Si and a-Si, it is worth noting that careful consideration is needed in terms of different situations. If the c-Si composition is high, greater emphasis is suggested to be paid on stronger mechanical adaptability, such as employing gradient structure or self-healing design to accommodate stronger anisotropic expansion. In the case of a-Si domination, the focus is proposed to be shift to better interface stability, such as optimizing SEI-forming pathway to ensure uniformity and tailoring thin-layer thickness with strong interfacial adhesion.

4.2.2 Percolation network integration. CNTs are widely recognized as high-efficiency conductive networks due to their superior electrical conductivity and mechanical properties compared to conventional carbon black. Notably, CNTs achieve better performance with a smaller addition amount, making them highly advantageous for silicon-based anodes. Among CNTs, single-walled CNTs (SWCNTs) have demonstrated a more pronounced impact on silicon-based anodes compared to multi-walled CNTs (MWCNTs). This is attributed to their higher aspect ratio, greater flexibility, and enhanced van der Waals interaction forces, which ensures better contact between the conductive network and active particles. In contrast, the relatively weak van der Waals forces of MWCNTs often result in poor electrical contact with active particles under lithiation stress during cycling, leading to rapid capacity decay (Fig. 4f).[39] *In situ* Raman spectroscopy provides further evidence of the superior performance of SWCNTs. When the lithiation degree exceeds 43%, two new peaks appear at 1485 cm^{-1} and 1460 cm^{-1}, corresponding to 14% and 16.5% strain, respectively, while the G-peak weakens significantly. Additionally, the emergence of two peaks at 1100 cm^{-1} and 980 cm^{-1}, corresponding to sp^3-edge carbon atoms and Si–C bonds, respectively, indicates the formation of interfacial chemical bonds between SWCNTs and lithiated Si clusters. This "mechanical–chemical" coupling reaction anchors pulverized Si clusters, preventing the formation of inactive "dead Si" and maintaining structural integrity. In contrast, MWCNTs, with their higher rigidity, do not exhibit such interfacial coupling reactions. As a result, they fail to suppress Si pulverization during cycling, leading to inferior performance compared to SWCNTs (Fig. 4g).[75] Furthermore, the length and aspect ratio of CNTs also significantly influence their overall performance as conductive networks. The structural and mechanical behavior of CNTs, particularly their compressive stress, SEI composition, and Li^+ diffusion

energy barrier, has been investigated for SWCNTs and MWCNTs with varying length-to-diameter ratios. Short, thick CNTs with high compressive stresses (on the gigapascal scale) are prone to penetrating the SEI and carbon coatings during the volume expansion of silicon anodes. This ''acupuncture effect'' accelerates electrolyte decomposition and increases the Li^+ diffusion energy barrier, thereby degrading performance. On the other hand, long, slender CNTs exhibit significantly lower compressive stress, which minimizes the acupuncture effect. This results in the formation of a thinner SEI layer and a reduced Li^+ diffusion barrier, enhancing overall electrochemical performance.[90] In summary, long SWCNTs emerge as the ideal conductive network for silicon-based anodes due to their unique combination of mechanical flexibility, high aspect ratio, and strong interfacial coupling with active materials. These characteristics ensure improved structural stability, minimized lithiation-induced stress, and enhanced Li^+ transport efficiency, making them a key component for advancing the performance of silicon-based lithium-ion batteries.

4.2.3 Functional binder design. The significant volume effect of micron-sized silicon-based anodes presents a critical challenge, necessitating the development of innovative multifunctional binders that can maintain mechanical stability without sacrificing overall electrical and ionic conductivity, even at low addition amounts. However, achieving this balance is highly challenging. The stress energy generated during lithiation/delithiation cycles is absorbed by the molecular motion of the cross-linked polymer binder within the electrode, leading to the formation of damage points on the covalent bonding network (CBN) of the binder. These damage points progressively worsen as alternating stress accumulates, eventually causing the electrode structure to collapse when the cumulative damage reaches the critical threshold of mechanical fatigue. Therefore, effectively dissipating energy to avoid damage accumulation within the binder network is essential to prevent binder fatigue failure.

A promising approach involves the ''mechanical interlocked network'' (MINs) strategy, exemplified by the design of the supramolecular binder DCMIN@PAA. This binder significantly enhances the structural stability of silicon-based anodes under high-stress conditions. The dynamic motion mechanism of the supramolecular polymer effectively dissipates the stress caused by volume expansion, preventing mechanical fatigue and damage accumulation commonly observed in traditional binders. Additionally, the dynamic host–guest recognition mechanism facilitates stress dissipation while reducing the formation of damage points within the binder network (Fig. 4h).[76] As a result, the Si-based anodes with the DCMIN@PAA binder achieve excellent cycling stability, maintaining a capacity retention rate of 71.9% even after 1050 cycles. Beyond its mechanical advantages, the DCMIN@PAA binder also demonstrates significant environmental benefits. Being water-soluble and degradable, it can be rapidly decomposed in alkaline aqueous solutions to enable the quick release and separation of active materials, offering an efficient and environmentally friendly solution for LIBs recycling. In the design of high-performance binders, mechanical reinforcement alone is insufficient; electronic and ionic conductivity must also be considered to achieve superior overall performance. New cross-linked composite binders can form a stable three-dimensional conduction network within the electrode, significantly enhancing the diffusion efficiency of ions and electrons. Unique doping characteristics enable these binders to maintain a stable doping state under working potentials, ensuring fast electron and ion transport during cycling.[91–93] However, while such innovative binder designs offer promising solutions, their manufacturing and recovery costs, as well as environmental impact, must also be carefully considered to ensure sustainable development and scalability.

The ICE of the micro-sized CVD-derived Si–C anodes in half cells currently ranges from 91% to 92%. However, prelithiation remains necessary to further compensate for irreversible lithium loss and improve the active lithium utilization rate of the cathodes. For this new class of anodes, the nano-sized silicon embedded within the porous carbon structure imposes stringent uniformity and controllability requirements for the prelithiation process. Several effective prelithiation strategies have been developed to address these challenges. Direct contact prelithiation using lithium foil is a simple and convenient method. However, this approach has two major drawbacks due to the use of thick lithium foils: the need to remove residual lithium metal after prelithiation and the occurrence of uneven prelithiation.[94] To mitigate these issues, thinning lithium layer techniques have been introduced as a promising solution. These techniques enable more uniform prelithiation and exhibit strong compatibility with industrial applications, making them highly suitable for large-scale implementation (Fig. 4i).[77,95,96] Chemical prelithiation has also been shown to improve the uniformity of lithiation. However, traditional lithiation reagents often have limited efficacy, necessitating the development of reagents with lower redox potentials to meet the demands of advanced anode designs.[97–99] The development of innovative chemical prelithiation reagents with high tolerance in air atmosphere and scalable potential has shown bright prospect.[100] Recently, a developed adhesion prelithiation strategy enabled by contact spontaneous lithium alloying reaction in a dry silicon-based anodes demonstrates good controllability, cost-effectivity, and industrial adaptability to cope with the high initial irreversible capacity loss in high loading situation. The ICE of all dry electrode-based full cells exceeds 98.73%, with the capacity retention rate after 300 cycles of 88.15%, shows great potential in scalable manufacturing of various high-capacity anodes.[101] Meanwhile, electrochemical prelithiation offers superior controllability, but its complex operational procedures significantly limit its feasibility for industrial-scale production.[102] As an emerging strategy, Li_2O with antifluorite structure and its derivatives, such as antifluorite compound Li_5FeO_4 (LFO), have good application prospects. Compared to Li_2O, the LFO compounds show the competitive capacity with significantly enhanced decomposition kinetics due to the decomposition potentials below 4.0 V (relative to Li/Li^+).[103–105] However, the unclear oxygen evolution mechanism of these compounds impedes the further practical application. Overall, chemical prelithiation and contact prelithiation, particularly with advancements in thinning lithium layer techniques,

demonstrate great potential for enhancing the electrochemical performance of micro-sized Si–C anodes. These methods strike a balance between controllability and cost-effectiveness, making them attractive for practical applications. Nevertheless, strict control of operational conditions during prelithiation remains essential to ensure consistent and reliable results.

5. Promoting practical performance of full cell with micro-sized CVD derived Si–C anodes under fast charging condition

In recent years, the development of high-performance LIBs has been characterized by two key trends: high-rate fast charging technology and increasing energy density. The rapid growth of the electric vehicle (EV) market has heightened consumer demand for extended driving range and expedited energy replenishment, making these areas a focal point for industry innovation. High-voltage fast-charging technology for high-energy-density LIBs represents a crucial strategy to enhance charging efficiency, substantially reduce charging time, and mitigate range anxiety. This has positioned fast-charging as an inevitable direction in LIBs technological advancement. Compared to conventional graphite anodes, micro-sized silicon-based anodes offer significant advantages, including their high theoretical capacity, which boosts overall energy density, and their relatively high lithiation potential, which mitigates the risk of lithium plating-induced safety hazards.[106] However, despite these benefits, silicon-based anodes have not yet been commercially adopted in fast-charging LIBs. This is primarily due to the severe pulverization caused by the immense stress that accumulates in silicon particles during lithiation. This stress leads to indiscriminate SEI growth and rapid capacity degradation. Additionally, silicon's intrinsic poor conductivity ($\sigma \approx 10^{-3}$ S cm^{-1} and $D_{Li^+} \approx 10^{-11}$ cm^2 s^{-1}) exacerbates the low diffusion efficiency, increasing polarization under fast-charging conditions.[107–109] *In situ* ^{7}Li NMR studies have provided valuable insights into the behavior of Si/lithium nickel cobalt manganese (NCM) oxides full cells during fast charging, revealing the rapid formation of Li_xSi and lithium plating at a 3C charging rate (Fig. 5a). Further spectral deconvolution in Fig. 5b illustrates the evolution of Li_xSi species during 3C charging. Notably, disordered Li_xSi resonances grow at a nearly constant rate, while ordered Li_xSi appears to plateau at a consistent intensity. This phenomenon is closely linked to the rate-limited lithiation of silicon. The kinetically limited surface reactions of silicon during fast charging lead to the formation of plated metallic lithium and the overlithiated $Li_{15+\delta}Si_4$ phase on and near the surfaces of silicon particles.[110] This issue becomes more pronounced with increasing particle size and charging rate, further contributing to performance degradation.

Recent studies have divided the lithiation kinetics of silicon into three distinct steps, as shown in Fig. 5c. Among these, the third phase transition results in the highest volume expansion, while the second step exhibits the fastest reaction rate. From

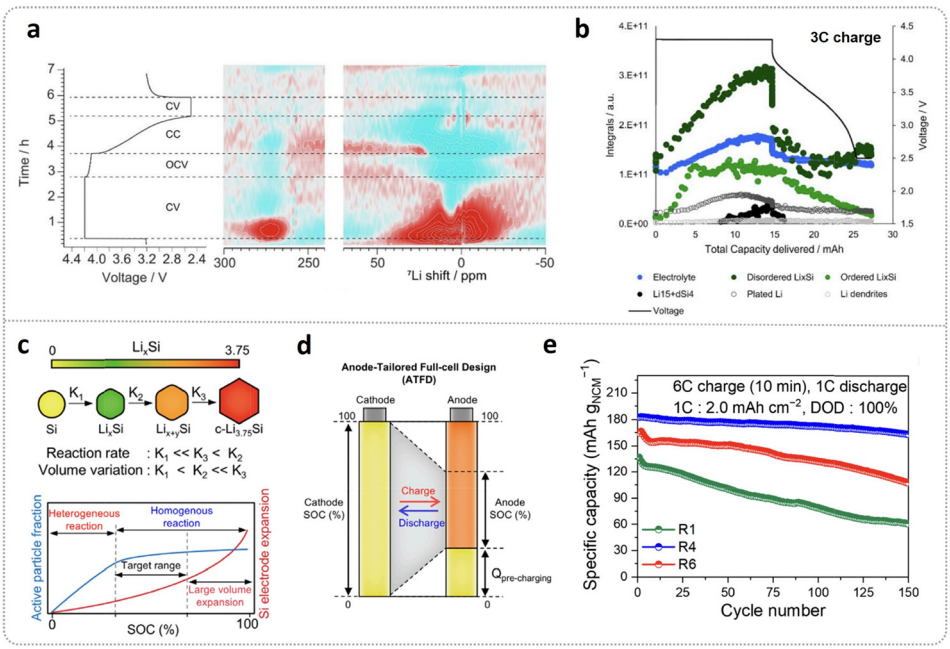

Fig. 5 Achieving fast-charging of full cell with micro-sized Si–C anodes. (a) Contour plots of the time derivative (dOp) of the operando ^{7}Li NMR intensities. (b) Capacity evolution of the integrals of the deconvoluted peaks corresponding to the responses from the ^{7}Li nuclei in various cell environments in the spectra from the operando ^{7}Li NMR experiment during the cycle with 3C charge,[110] with permission from American Chemical Society, 2023. (c) Reaction rate and volume variation during different lithiation stage of μ-Si and trends of active particle fraction and electrode expansion as a function of SOC. ATFD design (d) to achieve the high stability of μ-Si-based full cell under ultra fast charge (6C) and (e) corresponding cycling performance,[111] with permission from National Academy of Sciences, 2025.

the perspective of the relationship between reaction heterogeneity and volume expansion *versus* SOC, silicon volume expansion demonstrates a parabolic trend with increasing SOC, initially increasing rapidly before slowing down. Theoretically, operating silicon anodes at low SOC could minimize volume expansion. However, in practice, the low reaction kinetics at low SOC lead to high heterogeneity, causing significant capacity reduction. Consequently, operating within a moderate SOC range achieves an optimal balance between reaction kinetics and homogeneity. Based on this principle, an anode-tailored full-cell design (ATFD) has been proposed, as demonstrated in Fig. 5b. In this approach, the anode operates within a partial SOC range, while the cathode operates over the full SOC range. This asymmetric SOC operation enables the full cell to maintain excellent cycling stability even under extreme fast-charging conditions at a rate of 6C.[111] This work highlights the importance of balancing volume expansion and reaction kinetics across different lithiation stages of active materials. It also underscores the potential of designing customized operating protocols for high-volume-expansion anodes to meet the demands of fast charging. However, achieving superior performance under fast-charging conditions also requires matching innovative high-efficiency binders and carefully engineered electrolytes. These synergistic elements are critical for further improving the stability and efficiency of silicon-based fast-charging LIBs.

6. Summary and perspective

The micro-sized CVD-derived Si–C anode has garnered significant attention since its introduction, owing to its exceptional comprehensive performance in full cells. As a result, it has been recognized as the new generation of the "king of Si-based anodes." Additionally, its outstanding process economy further establishes it as one of the most promising ultimate solutions for high-energy-density LIBs. In this perspective, we first analyzed the differences in reaction pathways between c-Si and a-Si from the thermodynamic and kinetic aspects of phase transition. We then revisited the structural and interfacial failures of Si–C anodes, particularly examining the SEI "breathing" effect, to gain deeper insights into the performance degradation during prolonged cycling and storage. By focusing on the critical failure-inducing factors, we discussed potential strategies to enhance overall performance, including internal microstructure control and external regulation. Despite the significant progress achieved in improving the performance of micro-sized CVD-derived Si–C anodes through collaborative efforts from academia and industry, several challenges and limitations remain. Based on the current research landscape, the following aspects merit further attention and effort to accelerate the development of this technology:

(i) Considering the double-edged effects of modifications: no single modification strategy can comprehensively address all key performance issues. While certain approaches, such as the addition of FEC, effectively enhance cycling stability, they may have adverse effects on storage performance. Therefore, combining different modification strategies may provide better trade-offs between cycling life and calendar life, optimizing overall performance.

(ii) Focusing on internal interface issues: the nano-silicon embedded within the porous carbon skeleton introduces complex interfacial challenges. While significant progress has been made in quantifying and understanding the integrity of outer carbon coatings, the internal interfaces, such as the bonding strength, cracking, and detachment between nano-silicon and the carbon pores, remain poorly understood. Advanced monitoring and characterization techniques, including non-destructive testing technologies, are urgently needed to analyze the evolution and failure mechanisms occurring within the internal structure.

(iii) Customizing the pore structure of the carbon skeleton: the selection of precursors plays a decisive role in determining the synthesis route, application scenarios, and evaluation methodologies for the carbon skeleton. Different application scenarios impose varying requirements on pore size, pore volume, and porosity, which significantly influence the final anode performance. Beyond enhancing the understanding of the structure–activity relationship, it is critical to achieve precise regulation of pore characteristics tailored to specific application scenarios while ensuring product uniformity. This is essential for realizing high-performance anodes in practical applications.

(iv) Bridging the gap between academic research and industrial application: for commercialization, achieving consistent product performance is essential. This requires extensive experimental data supported by advanced simulation technologies to optimize manufacturing processes. Additionally, promoting low-cost silane-based processes combined with the development of new reactors can enhance the competitiveness and technical advantages of this production route, accelerating its industrial adoption.

In conclusion, micro-sized CVD-derived Si–C anodes represent a promising next-generation anode technology for high-energy-density LIBs. Over the past few years, these anodes have demonstrated exceptional performance and broad application prospects. Nevertheless, further advancements are urgently needed in calendar life, fast-charging capabilities, low-temperature discharge performance, and high-temperature cycling stability to accelerate their commercialization. We believe that with continued research efforts, particularly in understanding and addressing performance constraints in extreme environments, the commercialization of micro-sized CVD-derived Si–C anodes can be realized in the near future. By leveraging academic research to guide industrial development, this technology is poised to make a substantial impact on the next generation of LIBs.

Author contributions

Prof. Kang Xu and Prof. Lidan Xing performed the conceptualization, supervision and writing – review & editing. Prof. Weishan Li contributed to the resources and supervision. Zhexi Xiao performed the investigation, funding acquisition and

writing – original draft. Haojun Wu, Lijiao Quan and Fanghong Zeng, Ruoyu Guo, Zekai Ma, Xiaoyu Chen, Jiaqi Zhan contributed to the investigation and writing – original draft.

Data availability

No primary research results, software or code have been included and no new data were generated or analysed as part of this review.

Conflicts of interest

The authors declare no conflict of interest.

Acknowledgements

We would like to thank the financial support from the National Natural Science Foundation of China (22209095).

References

1 L. Sun, Y. Liu, L. Wang and Z. Jin, *Adv. Funct. Mater.*, 2024, **34**, 2403032.
2 M. Khan, S. Yan, M. Ali, F. Mahmood, Y. Zheng, G. Li, J. Liu, X. Song and Y. Wang, *Nano-Micro Lett.*, 2024, **16**, 179.
3 A. Brucker, A. Duran, N. P. Sullivan and A. Mistry, *ACS Energy Lett.*, 2024, **9**, 4053–4058.
4 Z. He, C. Zhang, Z. Zhu, Y. Yu, C. Zheng and F. Wei, *Adv. Funct. Mater.*, 2024, **34**, 2408285.
5 L. Yang, S. Li, Y. Zhang, H. Feng, J. Li, X. Zhang, H. Guan, L. Kong and Z. Chen, *J. Energy Chem.*, 2024, **97**, 30–45.
6 S. A. Ahad, T. Kennedy and H. Geaney, *ACS Energy Lett.*, 2024, **9**, 1548–1561.
7 N. Kim, Y. Kim, J. Sung and J. Cho, *Nat. Energy*, 2023, **8**, 921–933.
8 H. Li, H. Li, Y. Lai, Z. Yang, Q. Yang, Y. Liu, Z. Zheng, Y. Liu, Y. Sun, B. Zhong, Z. Wu and X. Guo, *Adv. Energy Mater.*, 2022, **12**, 2102181.
9 J. Wang, L. Liao, Y. Li, J. Zhao, F. Shi, K. Yan, A. Pei, G. Chen, G. Li, Z. Lu and Y. Cui, *Nano Lett.*, 2018, **18**, 7060–7065.
10 Z. Xiao, C. Yu, X. Lin, X. Chen, C. Zhang and F. Wei, *Carbon*, 2019, **149**, 462–470.
11 H. Zhang, L. Wang, H. Li and X. He, *ACS Energy Lett.*, 2021, **6**, 3719–3724.
12 M. Je, D.-Y. Han, J. Ryu and S. Park, *Acc. Chem. Res.*, 2023, **56**, 2213–2224.
13 L. Deng, Y. Zheng, X. Zheng, T. Or, Q. Ma, L. Qian, Y. Deng, A. Yu, J. Li and Z. Chen, *Adv. Energy Mater.*, 2022, **12**, 2200850.
14 J. Yan, C. Gao, S. Qi, Z. Jiang, L. R. Jensen, H. Zhan, Y. Zhang and Y. Yue, *Nano Energy*, 2022, **103**, 107779.
15 Z. Zhao, F. Chen, J. Han, D. Kong, S. Pan, J. Xiao, S. Wu and Q.-H. Yang, *Adv. Energy Mater.*, 2023, **13**, 2300367.
16 G. Zhu, D. Chao, W. Xu, M. Wu and H. Zhang, *ACS Nano*, 2021, **15**, 15567–15593.
17 Y. Gao, L. Fan, R. Zhou, X. Du, Z. Jiao and B. Zhang, *Nano-Micro Lett.*, 2023, **15**, 222.
18 J. Tao, L. Liu, J. Han, J. Peng, Y. Chen, Y. Yang, H.-R. Yao, J. Li, Z. Huang and Y. Lin, *Energy Storage Mater.*, 2023, **60**, 102809.
19 J. Wu, Q. Dong, Q. Zhang, Y. Xu, X. Zeng, Y. Yuan and J. Lu, *Adv. Mater.*, 2024, **36**, 2405751.
20 G. Xie, X. Tan, Z. Shi, Y. Peng, Y. Ma, Y. Zhong, F. Wang, J. He, Z. Zhu, X.-B. Cheng, G. Wang, T. Wang and Y. Wu, *Adv. Funct. Mater.*, 2024, **36**, 2414714.
21 N. Nitta, J. Tannaci and G. Yushin, *Ultra-Low Volume Change Silicon-Dominant Nanocomposite Anodes for Long Calendar Life and Cycle Life*, Sila Nanotechnologies, 2024.
22 I. Sehar, K. Shrivastava and A. Jain, *Int. J. Converging Technol. Manage*, 2024, **10**, 26–29.
23 A. Magasinski, P. Dixon, B. Hertzberg, A. Kvit, J. Ayala and G. Yushin, *Nat. Mater.*, 2010, **9**, 353–358.
24 M. Kim, Z. Yang and I. Bloom, *J. Electrochem. Soc.*, 2021, **168**, 010523.
25 J. Moon, B. Lee, M. Cho and K. Cho, *J. Power Sources*, 2014, **272**, 1010–1017.
26 J. W. Wang, Y. He, F. Fan, X. H. Liu, S. Xia, Y. Liu, C. T. Harris, H. Li, J. Y. Huang, S. X. Mao and T. Zhu, *Nano Lett.*, 2013, **13**, 709–715.
27 X. H. Liu, J. W. Wang, S. Huang, F. Fan, X. Huang, Y. Liu, S. Krylyuk, J. Yoo, S. A. Dayeh, A. V. Davydov, S. X. Mao, S. T. Picraux, S. Zhang, J. Li, T. Zhu and J. Y. Huang, *Nat. Nanotechnol.*, 2012, **7**, 749–756.
28 F. Fu, X. Wang, L. Zhang, Y. Yang, J. Chen, B. Xu, C. Ouyang, S. Xu, F.-Z. Dai and W. N. E, *Adv. Funct. Mater.*, 2023, **33**, 2303936.
29 H. Wu and Y. Cui, *Nano Today*, 2012, **7**, 414–429.
30 B.-K. Seidlhofer, B. Jerliu, M. Trapp, E. Hüger, S. Risse, R. Cubitt, H. Schmidt, R. Steitz and M. Ballauff, *ACS Nano*, 2016, **10**, 7458–7466.
31 M. Shimizu, K. Kimoto, T. Kawai, T. Taishi and S. Arai, *ACS Appl. Energy Mater.*, 2021, **4**, 7922–7929.
32 S. Cangaz, F. Hippauf, F. S. Reuter, S. Doerfler, T. Abendroth, H. Althues and S. Kaskel, *Adv. Energy Mater.*, 2020, **10**, 2001320.
33 J. Sakabe, N. Ohta, T. Ohnishi, K. Mitsuishi and K. Takada, *Commun. Chem.*, 2018, **1**, 24.
34 K. Zhao, M. Pharr, L. Hartle, J. J. Vlassak and Z. Suo, *J. Power Sources*, 2012, **218**, 6–14.
35 J. Hou, S. Qu, M. Yang and J. Zhang, *J. Power Sources*, 2020, **450**, 227697.
36 L. Sun, Y. Liu, R. Shao, J. Wu, R. Jiang and Z. Jin, *Energy Storage Mater.*, 2022, **46**, 482–502.
37 Y. Yin, E. Arca, L. Wang, G. Yang, M. Schnabel, L. Cao, C. Xiao, H. Zhou, P. Liu, J. Nanda, G. Teeter, B. Eichhorn, K. Xu, A. Burrell and C. Ban, *ACS Appl. Mater. Interfaces*, 2020, **12**, 26593–26600.
38 I. Yoon, J. M. Larson and R. Kostecki, *ACS Nano*, 2023, **17**, 6943–6954.
39 Z. He, Z. Xiao, H. Yue, Y. Jiang, M. Zhao, Y. Zhu, C. Yu, Z. Zhu, F. Lu, H. Jiang, C. Zhang and F. Wei, *Adv. Funct. Mater.*, 2023, **33**, 2300094.

40 Y. Wei, Z. Xiao, Y. Huang, Y. Zhu, Z. Zhu, Q. Zhang, D. Jia, S. Zhang and F. Wei, *Small*, 2024, **20**, 2310240.
41 Y. He, L. Jiang, T. Chen, Y. Xu, H. Jia, R. Yi, D. Xue, M. Song, A. Genc, C. Bouchet-Marquis, L. Pullan, T. Tessner, J. Yoo, X. Li, J.-G. Zhang, S. Zhang and C. Wang, *Nat. Nanotechnol.*, 2021, **16**, 1113–1120.
42 S. H. Kim, Y. S. Kim, W. J. Baek, S. Heo, D.-J. Yun, S. Han and H. Jung, *ACS Appl. Mater. Interfaces*, 2018, **10**, 24549–24553.
43 Q. Fang, S. Xu, X. Sha, D. Liu, X. Zhang, W. Li, S. Weng, X. Li, L. Chen, H. Li, B. Wang, Z. Wang and X. Wang, *Energy Environ. Sci.*, 2024, **17**, 6368–6376.
44 E. Wang, J. Wan, Y.-J. Guo, Q. Zhang, W.-H. He, C.-H. Zhang, W.-P. Chen, H.-J. Yan, D.-J. Xue, T. Fang, F. Wang, R. Wen, S. Xin, Y.-X. Yin and Y.-G. Guo, *Angew. Chem., Int. Ed.*, 2023, **62**, e202216354.
45 Y. Zhang, W.-P. Wang, Y. Zhao, X. Zhang, H. Guo, H. Gao, D.-X. Xu, Y.-M. Zhao, G. Li, J.-Y. Liang, S. Xin and Y.-G. Guo, *Adv. Funct. Mater.*, 2024, **34**, 2310309.
46 C. R. Lee, H. Y. Jang, H. J. Leem, M. A. Lee, W. Kim, J. Kim, J. H. Song, J. Yu, J. Mun, S. Back and H.-S. Kim, *Adv. Energy Mater.*, 2023, **14**, 2302906.
47 B. S. Lee, S.-H. Oh, Y. J. Choi, M.-J. Yi, S. H. Kim, S.-Y. Kim, Y.-E. Sung, S. Y. Shin, Y. Lee and S.-H. Yu, *Nat. Commun.*, 2023, **14**, 150.
48 B. Sreenarayanan, D. H. S. Tan, S. Bai, W. Li, W. Bao and Y. S. Meng, *J. Power Sources*, 2022, **531**, 231327.
49 M. Dubarry, N. Qin and P. Brooker, *Curr. Opin. Electrochem.*, 2018, **9**, 106–113.
50 J. D. McBrayer, M.-T. F. Rodrigues, M. C. Schulze, D. P. Abraham, C. A. Apblett, I. Bloom, G. M. Carroll, A. M. Colclasure, C. Fang, K. L. Harrison, G. Liu, S. D. Minteer, N. R. Neale, G. M. Veith, C. S. Johnson, J. T. Vaughey, A. K. Burrell and B. Cunningham, *Nat. Energy*, 2021, **6**, 866–872.
51 J. Sung, N. Kim, J. Ma, J. H. Lee, S. H. Joo, T. Lee, S. Chae, M. Yoon, Y. Lee, J. Hwang, S. K. Kwak and J. Cho, *Nat. Energy*, 2021, **6**, 1164–1175.
52 T. Lee, N. Kim, J. Lee, Y. Lee, J. Sung, H. Kim, S. Chae, H. Cha, Y. Son, S. K. Kwak and J. Cho, *Adv. Energy Mater.*, 2023, **13**, 2301139.
53 C. Yu, X. Chen, Z. Xiao, C. Lei, C. Zhang, X. Lin, B. Shen, R. Zhang and F. Wei, *Nano Lett.*, 2019, **19**, 5124–5132.
54 Z. Yan, S. Yi, Z. Wang, P. Ning, J. Zhang, J. Huang, Y. Xiao, D. Yang, Y. Zhang and N. Du, *Adv. Energy Mater.*, 2024, **14**, 2400598.
55 Y. Xiao, S. Yi, Z. Yan, X. Qiu, P. Ning, D. Yang and N. Du, *Small*, 2024, **20**, 2404440.
56 S. Park, J. Sung, S. Chae, J. Hong, T. Lee, Y. Lee, H. Cha, S. Y. Kim and J. Cho, *ACS Nano*, 2020, **14**, 11548–11557.
57 P. Xu, D. Guo, X. Lin, X. Wang, Z. Zhang, C. Zeng, M. Liao, Z. Su, Q. Huang and M. Zhang, *J. Energy Storage*, 2024, **98**, 113225.
58 S. Zhang, C. Liu, H. Wang, H. Wang, J. Sun, Y. Zhang, X. Han, Y. Cao, S. Liu and J. Sun, *ACS Nano*, 2021, **15**, 3365–3375.
59 Z. Li, Z. Zhao, S. Pan, Y. Wang, S. Chi, X. Yi, J. Han, D. Kong, J. Xiao, W. Wei, S. Wu and Q.-H. Yang, *Adv. Energy Mater.*, 2023, **13**, 2300874.
60 L. Zhang, J. Deng, L. Liu, W. Si, S. Oswald, L. Xi, M. Kundu, G. Ma, T. Gemming, S. Baunack, F. Ding, C. Yan and O. G. Schmidt, *Adv. Mater.*, 2014, **26**, 4527–4532.
61 Y. Li, F. Wu, Y. Li, X. Feng, L. Zheng, M. Liu, S. Li, J. Qian, Z. Wang, H. Ren, Y. Gong, C. Wu and Y. Bai, *Adv. Mater.*, 2023, **36**, 2310270.
62 Z. Yang, C. Wu, S. Li, L. Qiu, Z. Yang, Y. Zhong, B. Zhong, Y. Song, G. Wang, Y. Liu, Z. Wu and X. Guo, *Adv. Funct. Mater.*, 2021, **32**, 2107897.
63 Y. Wang, J. Song, H. Fan, Y. Luo, Z. Song, Y. Jin, S. Kim and W. Liu, *Energy Storage Mater.*, 2025, **74**, 103939.
64 Z. Zhu, Z. Pei, B. Liu, D. Sun, Y. Fang, X. Lei, X. Liu, S. Niu, H. Pan, J. Zhou, Y. Qian and G. Wang, *Adv. Funct. Mater.*, 2022, **32**, 2110444.
65 K. Ge, Z. Wang, J. Liu, Y. Mu, R. Wang, X. Xu, Y. Wang, Z. Zou, Q. Zhang, M. Han and L. Zeng, *Adv. Funct. Mater.*, 2025, **35**, 2414384.
66 W. Liu, L. Du, S. Ju, X. Cheng, Q. Wu, Z. Hu and X. Yu, *ACS Nano*, 2021, **15**, 5679–5688.
67 P. Zhou, P. Xiao, L. Pang, Z. Jiang, M. Hao, Y. Li and F. Wu, *Adv. Funct. Mater.*, 2025, **35**, 2406579.
68 S.-A. He, Q. Liu, Z. Cui, K. Xu, R. Zou, W. Luo and M. Zhu, *Small*, 2022, **18**, 2105866.
69 W. Feng, H. Wang, Y. Jiang, H. Zhang, W. Luo, W. Chen, C. Shen, C. Wang, J. Wu and L. Mai, *Adv. Energy Mater.*, 2022, **12**, 2103343.
70 K. Cheng, S. Tu, B. Zhang, W. Wang, X. Wang, Y. Tan, X. Chen, C. Li, C. Li, L. Wang and Y. Sun, *Energy Environ. Sci.*, 2024, **17**, 2631–2641.
71 Z. Xiao, X. Lin, C. Zhang, J. Shen, R. Zhang, Z. He, Z. Lin, H. Jiang and F. Wei, *Small Methods*, 2023, **7**, 2201623.
72 R. Zhang, Z. Xiao, Z. Lin, X. Yan, Z. He, H. Jiang, Z. Yang, X. Jia and F. Wei, *Nano-Micro Lett.*, 2023, **16**, 43.
73 S. Mao, J. Zhang, J. Mao, Z. Shen, Z. Long, S. Zhang, Q. Wu, H. Cheng and Y. Lu, *Adv. Energy Mater.*, 2024, **14**, 2401979.
74 Y. Deng, C. Li, R. Guo, Z. Xie, L. Huang, J. He, L. Xing and W. Li, *Adv. Funct. Mater.*, 2024, **35**, 2415820.
75 H. Wang, Y. Chao, J. Li, Q. Qi, J. Lu, P. Yan, Y. Nie, L. Wang, J. Chen and X. Cui, *J. Am. Chem. Soc.*, 2024, **146**, 17041–17053.
76 Z. Liu, Y. Wang, G. Liu, X. Yue, Z. Shi, Y. Tan, J. Zhao, Y. Lei, X. Yan and Z. Liang, *J. Am. Chem. Soc.*, 2024, **146**, 34491–34500.
77 C. Yang, H. Ma, R. Yuan, K. Wang, K. Liu, Y. Long, F. Xu, L. Li, H. Zhang, Y. Zhang, X. Li and H. Wu, *Nat. Energy*, 2023, **8**, 703–713.
78 Y. S. Meng, V. Srinivasan and K. Xu, *Science*, 2022, **378**, eabq3750.
79 D. J. Kautz, X. Cao, P. Gao, B. E. Matthews, Y. Xu, K. S. Han, F. Omenya, M. H. Engelhard, H. Jia, C. Wang, J.-G. Zhang and W. Xu, *Adv. Energy Mater.*, 2023, **13**, 2301199.
80 N. Zhang, T. Deng, S. Zhang, C. Wang, L. Chen, C. Wang and X. Fan, *Adv. Mater.*, 2022, **34**, 2107899.
81 Y. Peng, C. Zhong, M. Ding, H. Zhang, Y. Jin, Y. Hu, Y. Liao, L. Yang, S. Wang, X. Yin, J. Liang, Y. Wei, J. Chen, J. Yan, X. Wang, Z. Gong and Y. Yang, *Adv. Funct. Mater.*, 2024, **34**, 2404495.

82 J. Quinn, J.-M. Kim, R. Yi, J.-G. Zhang, J. Xiao and C. Wang, *Adv. Mater.*, 2024, **30**, 2402625.
83 H. Shin, J. Park, A. M. Sastry and W. Lu, *J. Electrochem. Soc.*, 2015, **162**, A1683.
84 K. Kalaga, M.-T. F. Rodrigues, S. E. Trask, I. A. Shkrob and D. P. Abraham, *Electrochim. Acta*, 2018, **280**, 221–228.
85 Y. Yang, Z. Yang, Z. Li, J. Wang, X. He and H. Zhao, *Adv. Energy Mater.*, 2023, **13**, 2302068.
86 Z. Cao, X. Zheng, Q. Qu, Y. Huang and H. Zheng, *Adv. Mater.*, 2021, **33**, 2103178.
87 G. Liu, M. Xia, J. Gao, Y. Cheng, M. Wang, W. Hong, Y. Yang and J. Zheng, *ACS Appl. Mater. Interfaces*, 2023, **15**, 3586–3598.
88 Y. Ko, J. Bae, G. Chen, M. A. Baird, J. Yan, L. Klivansky, D.-M. Kim, S. E. Trask, M.-T. F. Rodrigues, G. M. Carroll, N. R. Neale and B. A. Helms, *ACS Energy Lett.*, 2024, **9**, 3448–3455.
89 J. Langdon, R. Sim and A. Manthiram, *ACS Energy Lett.*, 2022, **7**, 2634–2640.
90 Z. He, C. Zhang, Y. Zhu and F. Wei, *Energy Environ. Sci.*, 2024, **17**, 3358–3364.
91 Y. Yu, C. Yang, J. Zhu, B. Xue, J. Zhang and M. Jiang, *Angew. Chem., Int. Ed.*, 2024, **64**, e202418794.
92 Y. Yu, C. Yang, Y. Jiang, J. Zhu, J. Zhang and M. Jiang, *Nano Energy*, 2024, **130**, 110108.
93 Y. Yu, J. Zhu, Y. Li, Q. Xu, Y. Jiang, C. Yang, L. Shi, L. Chen, P. Liu, J. Zhang and M. Jiang, *Chem. Eng. J.*, 2024, **479**, 147807.
94 M. Gautam, G. K. Mishra, A. Ahuja, S. Sau, M. Furquan and S. Mitra, *ACS Appl. Mater. Interfaces*, 2022, **14**, 17208–17220.
95 C. Wang, F. Yang, W. Wan, S. Wang, Y. Zhang, Y. Huang and J. Li, *Energy Environ. Sci.*, 2023, **16**, 4660–4669.
96 H. Wang, M. Zhang, Q. Jia, D. Du, F. Liu, M. Bai, W. Zhao, Z. Wang, T. Liu, X. Tang, S. Li and Y. Ma, *Nano Energy*, 2022, **95**, 107026.
97 H. Shen, Y. An, Q. Man, J. Wang, C. Liu, B. Xi, S. Xiong, J. Feng and Y. Qian, *Chem. Eng. J.*, 2023, **454**, 140136.
98 X. He, X. Mu, Y. Wang, P. Wang and P. He, *ACS Appl. Energy Mater.*, 2023, **6**, 6790–6796.
99 L. Quan, Q. Su, H. Lei, W. Zhang, Y. Deng, J. He, Y. Lu, Z. Li, H. Liu, L. Xing and W. Li, *Natl. Sci. Rev.*, 2025, nwaf084.
100 Y. J. Gao, C. H. Cui, Z. K. Huang, G. Y. Pan, Y. F. Gu, Y. N. Yang, F. Bai, Z. Sun and T. Zhang, *Angew. Chem., Int. Ed.*, 2024, **136**, e202404637.
101 H. Dong, T. Yang, C. Liu, D. Luo, N. Liu, Y. Gao, Z. Shi, Y. Zhang and Z. Chen, *Energy Storage Mater.*, 2025, **75**, 104072.
102 L. Ünal, V. Maccio-Figgemeier, L. Haneke, G. G. Eshetu, J. Kasnatscheew, M. Winter and E. Figgemeier, *Adv. Mater. Interfaces*, 2024, **11**, 2400024.
103 Y. Chen, Y. Zhu, W. Zuo, X. Kuai, J. Yao, B. Zhang, Z. Sun, J. Yin, X. Wu and H. Zhang, *Angew. Chem., Int. Ed.*, 2024, **136**, e202316112.
104 W. Lee, H. Lee, Y. Byeon, J. H. Kim, W. Choi, M. Choi, M.-S. Park and W.-S. Yoon, *Adv. Energy Mater.*, 2023, **13**, 2302316.
105 Y. Zhu, R. Xu, Y. Zheng, Y. Chen, J. Yin, J. Xue, B. Zhang, L. Li, G. Zeng and H. Luo, *Angew. Chem., Int. Ed.*, 2025, e202502126.
106 N. Kim, S. Chae, J. Ma, M. Ko and J. Cho, *Nat. Commun.*, 2017, **8**, 812.
107 Q. Li, R. Yi, Y. Xu, X. Cao, C. Wang, W. Xu and J.-G. Zhang, *J. Power Sources*, 2022, **548**, 232063.
108 K. Pan, F. Zou, M. Canova, Y. Zhu and J.-H. Kim, *J. Power Sources*, 2019, **413**, 20–28.
109 J. He, J. Meng and Y. Huang, *J. Power Sources*, 2023, **570**, 232965.
110 K. J. Sanders, A. A. Ciezki, A. Berno, I. C. Halalay and G. R. Goward, *J. Am. Chem. Soc.*, 2023, **145**, 21502–21513.
111 T. Lee, M. J. Seong, H. C. Ahn, M. Baek, K. Park, J. Oh, T. Choi and J. W. Choi, *Proc. Natl. Acad. Sci. U. S. A.*, 2025, **122**, e2417053121.

